Investigation on Dry Spinning Process of Ultrahigh Molecular Weight Polyethylene/Decalin Solution

Yushan Sun,[1,2] Qingrui Wang,[2] Xiaojun Li,[1] Xueying Chen,[2] Yan Ma,[1] Qi Zhang,[1] Xiaofang Jin,[1] Yuan Jiang,[1] Lin Sun,[1] Qiang Luo[1]

[1]*College of Materials Science and Engineering, Donghua University, Shanghai 200051, People's Republic of China*
[2]*Research and Development Center, China Textile Academy, Beijing 100025, People's Republic of China*

Received 2 October 2004; accepted 18 January 2005
DOI 10.1002/app.22001
Published online in Wiley InterScience (www.interscience.wiley.com).

ABSTRACT: The relationship between the draw-down ratio in the dry spinning process of ultrahigh molecular weight polyethylene/decalin solution and the fiber performance through maximized after-drawing was investigated. The structural development during the after-drawing process was analyzed by scanning electron microscopy, differential scanning calorimetry, wide-angle X-ray diffraction, sonic velocity, and FTIR measurements. An optimum draw-down ratio was found in the multihole dry spinning process, which may be explained by molecular disentanglement and the composite effect of entropy and the viscosity component. The as-spun fiber by draw-down had an obvious shish kebab morphology, lower crystallinity, and a higher melting temperature compared with a free extrusion sample, and higher crystallinity and melting temperature compared with the fiber by first-stage after-drawing. During the subsequent after-drawing process, the crystallinity, melting temperature, X-ray diffraction, and sonic velocity orientation factors increased slowly in the higher after-drawing ratio region, which was not consistent with the rising tendency of the tensile properties. The polarized and unpolarized IR spectra reflected the variations of the orientation and the content of the folded chains. © 2005 Wiley Periodicals, Inc. J Appl Polym Sci 98: 474–483, 2005

Key words: high performance polyethylene fiber; extrusion; drawing; orientation; structure–property relations

INTRODUCTION

Of to the technological routes for high performance polyethylene (PE) fibers, the dry spinning process of ultrahigh molecular weight PE (UHMWPE)/decalin solution has become very important in industrial production[1] because of its low cost, good fiber properties, and environmental considerations. It is meaningful to obtain a better understanding about this special dry spinning process. When decalin is adopted as a solvent for UHMWPE, it is so volatile that it is easily volatilized far below its boiling point. This character is needed, because high temperature drying is unfavorable for solution spun UHMWPE fiber (in that case, the drawability will be as poor as melt spun fiber).[2,3] Molecular entanglement is a main problem faced in producing high performance PE fibers from UHMWPE.[4–6] A low polymer concentration of the spinning dope may reduce the entanglements,[7] but the theoretical concentration for suitable entanglements[8] is too low to ensure extrusion equality in a multihole spinneret (because of the low viscosity and pressure upon the spinneret). For such a reason, the molecular disentanglement of a higher concentration spinning dope after extrusion is necessary for the control of the total effective drawability and fiber performance in the multihole spinning process. In recent years, there has been much patent literature about control of the draw-down process for industrial production.[9,10] For the after-drawing process of as-spun UHMWPE fiber, several groups reported that the traditional supermolecular structural parameters, such as the crystallinity, X-ray diffraction (XRD) orientation factor (f_x), and sonic velocity orientation factor (f_s), could not explain the relationship between the fiber performance (tensile strength, modulus) and draw ratio in the higher draw ratio range, because the tensile strength and modulus of UHMWPE fibers increased with increasing draw ratio in the whole range, but the crystallinity, f_x, and f_s increased very slowly (tending to a plateau value) in the higher draw ratio range.[11–16] Some reports tried to explain these by the fraction of extended chain crystals[16] or fibrillar materials[17] derived from the differential scanning calorimetry (DSC) peak of the orthorhombic–hexagonal phase transition.[18–20] In this article, experiments about the relationship between the draw-down ratio (λ_{ext}; spinneret draft) in the draw-down process of dry spinning of UHMWPE/decalin solution and the fiber performance (through maximized after-drawing) were performed and the results of the "peak phenomenon" are discussed based

Correspondence to: Y. Sun (sunys@cta.com.cn).

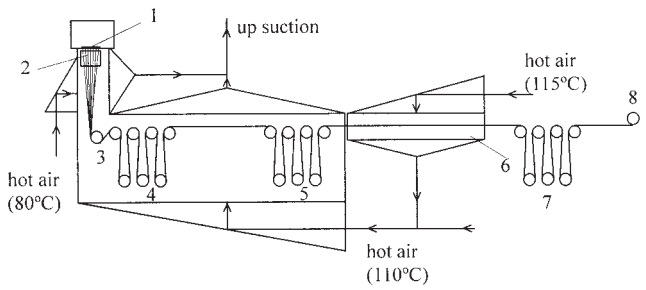

Figure 1 The diagram of the spinning process: (1) spinneret, (2) spinning line oven, (3) guide roller, (4) first seven-roller machine, (5) second seven-roller machine, (6) draw box, (7) third seven-roller machine, and (8) winder.

on a two-component (entropy and viscosity) model. The relationship between the fiber performance and the after-drawing ratio in the after-drawing process was investigated by scanning electron microscopy (SEM), DSC, wide-angle XRD (WAXD), sonic velocity, and FTIR tests.

EXPERIMENTAL

The decalins used in the experiments were industrial grade chemicals (*trans*-decalin 76%, bp 195°C; *cis*-decalin 24%, bp 187°C). In the experiments (hereafter noted as experimental series 1) about the relationship between the λ_{ext} (spinneret draft) in the draw-down process and the maximized fiber performance through after-drawing, 7.8 wt % of UHMWPE powder (GUR 412, weight-average molecular weight = 3×10^6) was dissolved in decalin and stabilized by 0.5 wt % of the antioxidant 2,6-di-*t*-butyl-4-methyl-cresol. The decalin, antioxidant, and PE powder were charged into a swelling kettle, and the mixture was heated with fast agitation to 95–97°C. The PE polymer was swollen at 95–97°C for 1 h, and then the suspension slurry of PE was fed to a corotating twin-screw extruder. The temperature distribution of the heating zones for the twin-screw extruder was 108–180°C, and its end pressure was 2.95 MPa. The temperature distribution of the heating zones from the twin-screw extruder to the booster pump to the prefilter to the spinning trunk was from 180 to 190°C, and the pressure of the spinning pack was 0.43 MPa. The PE was dissolved in decalin and at the same time deaerated as it traversed the extruder. From the twin-screw extruder to the spinning trunk, the spinning dope passed through every heating zone and then into the spinning gear pump. The spinning dope was then pumped through a 174-hole spinneret. Two kinds of spinnerets [1 mm with a 10/1 length/diameter (L/D) ratio or 0.6 mm with 6/1 L/D] were used for comparison. Figure 1 shows the diagram of the spinning process. The extrusion speed was fixed to 1.5 m/min, and the draw-down speed was changed to attain different λ_{ext} values. At the 2-cm position under the spinneret, there was a temperature controlled cylindrical oven with a center temperature of 155°C and a 30-cm length. When the extruded thread line went out of the spinning line oven, it was immediately blown by a 80°C cross air flow (~0.8 m/s) coming from a lateral blow window screen; then, it went through a guide roller. The vertical distance from the spinneret to the guide roller was 1.6 m. The filaments then ran horizontally from the guide roller to the first and second seven-roller machines, which were included in a 4 m long drying case. The hot air from the outlet of the subsequent draw box (~110°C) came from the bottom window screen of the case (~1.5 m/s), and there was a centrifuge fan for the up-suction from the case and the lateral blow window screen. The temperature of the second seven-roller machine was 95°C for preheating of the successive drawing. The temperature of the draw box was 115°C (hot air flow from the top window screen), and the filaments were drawn in the draw box between the second and third seven-roller machines; then, they were wound up on the bobbin for the next drawing. For measuring the residual decalin of different processing positions, the filament samples were taken from the position of the guide roller, the end of the second seven-roller machine, and the windup bobbin. The samples were immediately put in sealed containers and weighed. After wet weighing, the samples were removed and placed in the vacuum drying oven (0.08-MPa vacuum) with the temperature controlled at 78–80°C. Then, they were weighed until the weight (W) was constant (dry weight). The volatility (V) of decalin was calculated from eq. (1):

$$V = \left(1 - \frac{W_{wet} - W_{dry}}{W_{dry} \times n}\right) \times 100\% \qquad (1)$$

where n was equal to $W_{decalin}/W_{PE}$ in the spinning dope. The results were as follows: V(guide roller position) = 65.15%, V(end of the second seven-roller machine position) = 99.76%, and V windup bobbin position) = 99.98%.

For the after-drawing process subsequent to the draw-down, first-stage drawing [draw ratio (λ_1)] was included in the spinning process as mentioned above in a 2 m long draw box (hot air flow, middle position temperature = 115°C) before take-up, and λ_1 was determined by the breaking draw ratio (0.8 $\lambda_{breaking}$). The second- and third-stage drawing were undertaken in the next separate process (see Fig. 2). The feeding speed was 1 m/min and the feeding roll temperature was 80°C. The second-stage drawing was in a 4 m long draw box (hot air circulation flow, entrance temperature = 135°C, exit temperature = ~132°C), and the draw ratio (λ_2) was also determined by 0.8 $\lambda_{breaking}$.

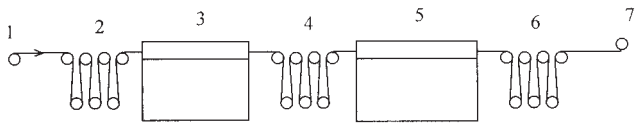

Figure 2 The diagram of the after-drawing process: (1) bobbin from the spinning process, (2) seven-roller machine for feeding, (3) hot draw box for draw ratio (λ_2), (4) seven-roller machine for λ_2 drawing, (5) hot draw box for draw ratio (λ_3), (6) seven-roller machine for λ_3 drawing, and (7) winder.

The third-stage drawing was in a 5 m long draw box (hot air circulation flow, entrance temperature = 143°C, exit temperature = ~139°C), and the draw ratio (λ_3) was determined by 0.9 $\lambda_{breaking}$. In the above-mentioned multistage drawing, all draw rolls (except the feeding roll) were at room temperature. The thus obtained fiber samples were taken for performance (tensile strength, modulus) testing.

In the experiments (hereafter noted as experimental series 2) to determine the relationship between the fiber performance and the after-drawing ratio in the after-drawing process, 6% (w/v) UHMWPE powder (viscosity-average molecular weight = 4.6×10^6, polydispersity = 4.67, branching content = 1.53 —CH_3/1000C, commercial product, Beijing Auxilliaries Plant No. 2, Beijing) was dissolved in decalin. The dissolving process and the spinning line oven were basically the same as mentioned before. The spinning dope was pumped through a 364-hole spinneret and each hole of the spinneret was 0.6-mm diameter and 6/1 L/D. The extrusion speed was 1.7 m/min and the λ_{ext} was 5.9. When the extruded thread line went out of the spinning line oven, it was immediately blown by a 80°C cross N_2 gas flow coming from a lateral blow window screen; then, it went through an 8 m high vertical duct with the 115–80°C N_2 gas flowing from the lower part to the upper part. For the after-drawing process subsequent to the draw-down, first-stage drawing (λ_1 = 4.0) was included in the spinning process in a 4 m long draw box (hot air circulation flow, 115°C). The second- to fourth-stage drawings were undertaken in the next separate process. The feeding speed was 2 m/min and the feeding roll temperature was 80°C. The second-stage drawing was in an 8 m long draw box (hot air circulation flow, 130°C) and the λ_2 was 3.75. The third-stage drawing was in an 8 m long draw box (hot air circulation flow, 135°C) and the λ_3 was 1.307. The fourth-stage drawing was in an 8 m long draw box (hot air circulation flow, 140°C) and the draw ratio (λ_4) was 1.18. After the fourth-stage drawing, the filaments passed through a relaxation seven-roller machine and then were wound up with a winding tension of 190 cN/364 filaments.

The tensile properties of UHMWPE fibers were determined at room temperature using an Instron tensile tester (model 1122). The testing speed was 12 mm/min and the clamp distance was 88 mm. The tensile strength, initial modulus, and elongation at break were calculated according to the JIS L1013-1992 standard.

SEM micrographs were obtained from the detection of backscattered electrons or the mixing detections of backscattered and secondary electrons with an XL-30 scanning electron microscope (FEI Co. Ltd.). The samples were covered with a gold layer to prevent electric charging.

The DSC thermograms were measured by using a Perkin–Elmer Pyris 1 DSC differential scanning calorimeter at a heating rate of 5°C/min in a nitrogen atmosphere. An indium standard was used for temperature calibration with an empty sample pan as the reference. The samples were cut into pieces of 2–3 mm in length. Scans were conducted from 60 to 180°C.

The WAXD tests of the fibers were carried out using a Rigaku D/MAX-rA X-ray diffractometer with nickel-filtered Cu Kα radiation (wavelength = 1.5406 Å). The filaments were mounted parallel on a flat sample frame for equatorial, meridional, and azimuthal scans.

The orientation factor of the sonic velocity was determined by measuring the transit time of a sound pulse between two transducers coupled to the specimens. The measurements were made by using a SSY-I model fiber sonic velocity meter. From the measured sonic velocity (C), the orientation factor of the samples (f_s) was calculated from eq. (2):

$$f_s = 1 - (C_u/C)^2 \quad (2)$$

where C_u is the sonic velocity of the fully unoriented sample, which is 1.40 km/s.[21]

The polarized or unpolarized IR spectra were measured by using a Nicolet Impact 400D FTIR spectrometer with a spectral resolution of 4 cm^{-1}.

RESULTS AND DISCUSSION

Figures 3 and 4 present the relationships between the λ_{ext} (spinneret draft) in the draw-down process of the dry spinning of UHMWPE/decalin solution and the fiber performance (tensile strength; modulus, through maximized after-drawing). Note that each of the fiber performance/draw-down ratio relationship curves shows a peak, and the draw-down ratios corresponding to the peaks are different from each other for different hole diameters and length/diameter ratios. This peak phenomenon is in accordance with the patent publications about the control of the draw-down process of UHMWPE solution in recent years.[9,10] According to widely approved viewpoints, the drawability of the as-spun UHMWPE fiber and the fiber performance through maximized after-drawing largely depend on the molecular entanglements,[3,5,6,22]

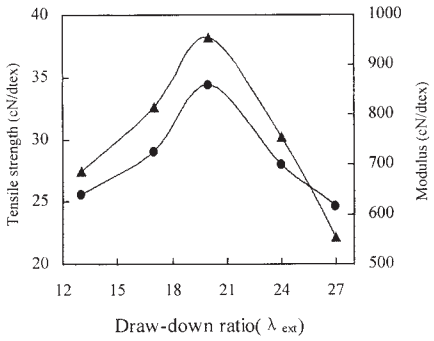

Figure 3 The (●) tensile strength and (▲) modulus of UHMWPE fibers (after maximized after-drawing) versus the draw-down ratio (experimental series 1, hole diameter = 1 mm, length/diameter ratio = 10).

so there might be some kind of correlation between the draw-down ratio and the molecular disentanglement. We discuss this based on the two- component model in Figure 5, where the Hookean spring in the Voight–Kelvin viscoelastic model is represented by the entropy component (σ_e; the retractive force from the spontaneous increase of entropy). As the pseudoplastic behavior of polymer fluid has been effectively interpreted by the conformational variation of macromolecules and molecular entanglements,[23] we separate the above factors from the linear component of the Newtonian viscosity:

$$\sigma = \sigma_v + \sigma_c \tag{3}$$

$$\sigma_v = \eta\dot{\varepsilon} \tag{4}$$

where η represents the Newtonian viscosity and $\dot{\varepsilon}$ is the strain rate, which is given by

$$\dot{\varepsilon} = \frac{\partial V_x}{\partial X} = \frac{V - V_0}{L} = \frac{V_0}{L}(\lambda - 1) \tag{5}$$

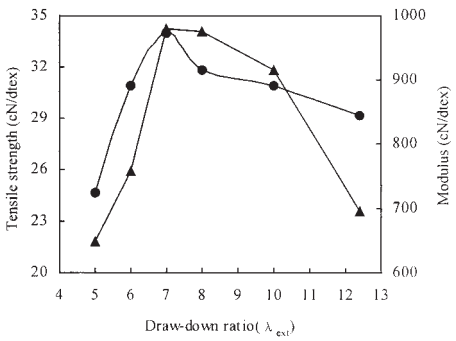

Figure 4 The (●) tensile strength and (▲) modulus of UHMWPE fibers (after maximized after-drawing) versus the draw-down ratio (experimental series 1, hole diameter = 0.6 mm, length/diameter ratio = 6).

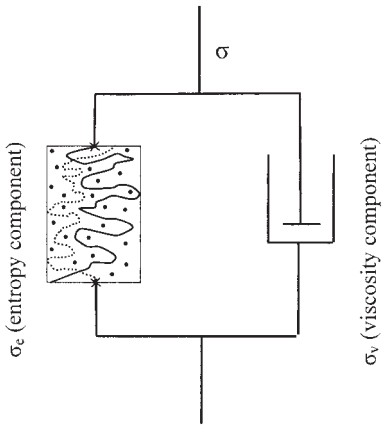

Figure 5 The two-component model for the draw-down process: (●) chains perpendicular to the paper plane, (×) highly tangled and equivalently fixed link, and (- - -, —) two macromolecules.

where V is the draw-down speed, V_0 is the extrusion speed, and L is the length of the strain region. The value of σ_e can be derived from the entropy and free energy analysis[24–26] in eq. (6):

$$\sigma_e = N_c kT\frac{D}{1-\alpha^2\phi}\left(\frac{1-\alpha^2}{1-\alpha^2\phi} - \alpha^2\right) + N_s kT\left\{\frac{(1-\alpha^2)(1+\beta)}{1-\alpha^2\phi}\left[\frac{\alpha^2 D}{1-\alpha^2\phi}\left(\frac{\lambda^2}{1+\beta\lambda^2} + \frac{2}{\lambda+\beta}\right) + \frac{\lambda}{(1+\beta\lambda^2)^2} - \frac{1}{(\lambda+\beta)^2}\right] + \beta\left[\frac{\lambda}{1+\beta\lambda^2} - \frac{1}{\lambda(\lambda+\beta)}\right] - \frac{\alpha^2 D}{1-\alpha^2\phi}\right\} \tag{6}$$

where

$$D = \lambda - 1/\lambda^2 \tag{7}$$

$$\phi = \lambda^2 + 2/\lambda \tag{8}$$

where N_c and N_s represent the number of crosslinks (highly tangled and equivalently fixed links) and sliplinks per unit volume, respectively; λ is the draw-down ratio; k is the Boltzmann constant; T is the absolute temperature; α is the measure of inextensibility; and β is the measure of slippage (the degree of sliplink freedom). Qualitatively analyzing, at higher temperature and a certain $\dot{\varepsilon}$, the η will decrease, so σ_v will be smaller, which will make the slippage of the molecular chain easier. At the same time σ_e will increase because of the higher T value, which makes the extension of the molecular chain more difficult. The multiple effect of the above will be in favor of the disentanglement of slightly tangled links. As for the same temperature, lower $\dot{\varepsilon}$ will also make σ_v smaller,

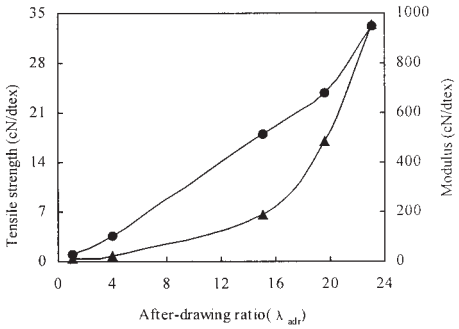

Figure 6 The (●) tensile strength and (▲) modulus of UHMWPE fibers (samples from experimental series 2) versus the after-drawing ratio.

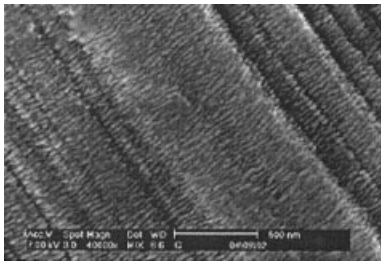

Figure 7 A scanning electron micrograph based on the mixture of secondary electrons and backscattered electrons for the UHMWPE fiber (draw-down sample from experimental series 2) with $\lambda_{ext} = 5.9$ ($\lambda_{adr} = 1$); original magnification ×40,000.

and thus advantageous for slippage and disentanglement. However, because the entanglement links form a kind of transient network in the dynamic state, too low a strain rate will be ineffective for disentanglement because of Brownian movement. In contrast, if the $\dot{\varepsilon}$ is too high, the slippage will be more difficult because of the high viscous force σ_v and meanwhile local disorder will be brought about from excessive taut entanglements, which will behave as permanent structural defects in the following after-drawing steps. The $\dot{\varepsilon}$ can be adjusted by V_0, L, or λ. As for λ, too low a λ value will be insufficient for disentanglement, and too high a λ value will tend to bring about the structural defects as in the case of excessively high $\dot{\varepsilon}$. The different λs, corresponding to the peaks between Figure 1 and Figure 2, may be mainly attributed to the die swell caused by different spinneret hole diameters and hole length/diameter ratios.

Figure 6 shows the relationship between fiber performance and the after-drawing ratio in the after-drawing process of experimental series 2. In this series the after-drawing ratios (λ_{adr}) of 4, 15, 19.6, and 23.1 corresponded to drawing temperatures (last step for each sample) of 115, 130, 135, and 140°C, respectively, whereas the sample with a λ_{adr} of 1 was the draw-down sample ($\lambda_{ext} = 5.9$). The structural development in the UHMWPE fibers during this after-drawing process was then analyzed by a series of tests. Figure 7 shows the obvious shish kebab morphology of the draw-down sample, and the progressive extending process of folded chains is presented in Figures 7–9. Figures 10 and 11 provide the unconstrained and constrained DSC thermograms of fiber samples with different λs (λ_{adr}). The constrained DSC thermograms have been used for research on the orthorhombic–hexagonal phase transition (O—H transition) of solution spun and ultradrawn UHMWPE fibers or films.[3,11,18–20,27–32] The O—H transition, which is commonly found in odd *n*-paraffins a few degrees below the melting point,[33,34] has been observed in PE in crosslinked samples,[34,35] in samples under hydrostatic pressure or reactor powder extrusion drawn samples,[36,37] and upon constrained heating of UHMWPE shish kebab fibers produced by the "surface growth" technique[28] or solution spun and ultradrawn UHMWPE fibers or films. In all cases the appearance of the hexagonal phase in PE can be attributed to strong restrictions experienced by the molecules in the adoption of a random coil conformation, which is attributable to the presence of chemical crosslinks, the reduction of the free volume under high pressure, and very effective entanglements in high molecular weight material. Especially if the molecules are fully extended between these entanglements in the UHMWPE fibers, an O—H transition may be expected, because recoiling would require slippage of the molecules throughout the entanglements, which cannot occur if the molecular network is kept at constant length.[18] It has been proved that, at normal temperature, there is no detectable hexagonal phase in the ultradrawn UHMWPE fiber or film but, at high temperature and in a constrained state, the O—H transition can be detected by DSC, WAXD, or FTIR.[3,11,18–20,27–32] For instance,[19] it was found by DSC, time-resolved WAXD, and FTIR that there were two endothermic peaks between 146 and 154°C, which respectively correspond to the transitions from the orthorhombic phase to the hexagonal phase and to the melt. As the temperature was in-

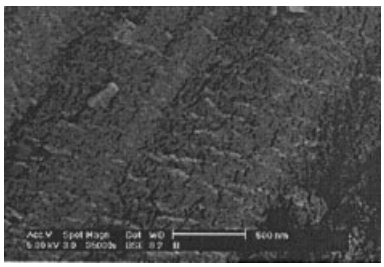

Figure 8 A scanning electron micrograph based on the backscattered electrons for the UHMWPE fiber (after-drawing sample from experimental series 2) with $\lambda_{adr} = 4$; original magnification ×35,000.

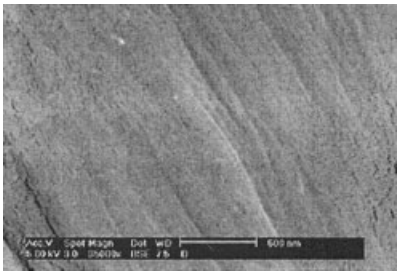

Figure 9 A scanning electron micrograph based on the backscattered electrons for the UHMWPE fiber (after-drawing sample from experimental series 2) with λ_{adr} = 15; original magnification ×35,000.

creased to the phase transition region detected in the DSC thermograms, the intensities of the 110 and 200 reflections of the orthorhombic phase decreased and the 100 reflection of the hexagonal phase began to appear. With further increase of the temperature, the orthorhombic phase disappeared finally and the hexagonal phase increased its intensity. In the higher temperature region, the reflection pattern gradually changed to the halo characteristic of the molten state. The integrated intensity of the 1471 cm^{-1} IR absorption band (orthorhombic crystalline band) decreased and the 1466 cm^{-1} band (hexagonal crystalline band) increased in the temperature region where the O—H transition was detected in the DSC curve.[19] Figures 10 and 11 show that, for free extrusion and samples with a λ_{adr} value of 1 (λ_{ext} = 5.9), single melting peaks were observed in both unconstrained and constrained states. The endothermic curves moved slightly in the higher temperature direction for the constrained state or for the sample with a λ_{adr} of 1 in the same state. For the λ_{adr} 4 sample, the endothermic curve in the unconstrained state was broader and more symmetric and in the constrained state two peaks were observed. This is because as long as the molecules are not fully

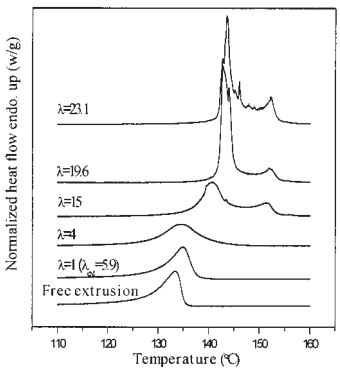

Figure 10 Unconstrained melting endotherms recorded at a scan speed of 5°C/min in the DSC of UHMWPE fibers (samples from experimental series 2) with various after-drawing ratios.

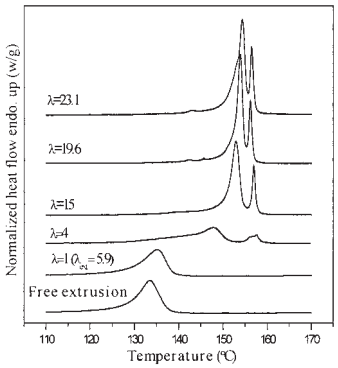

Figure 11 Constrained melting endotherms recorded at a scan speed of 5°C/min in the DSC of UHMWPE fibers (samples from experimental series 2) with various after-drawing ratios.

elongated between entanglements, as is the case in the kebabs, they can randomize and melt as in the unconstrained state. However, for the molecules that have become fully taut between entanglements, no randomization seems to occur in the time scale of the experiment and, instead of melting, the orthorhombic lattice transforms into the hexagonal phase.[18–20] The first peak temperature of the λ_{adr} 4 sample in Figure 11 was distinctly lower (147.7°C) than those of other samples with higher λ_{adr} (152.9–154.3°C for λ_{adr} = 15–23.1). This might be related to the lower molecular taut extent between entanglements, and the endotherm seemed to be a mixture of melting and orthorhombic–hexagonal phase transition. The second peak temperatures in Figure 11 were basically the same (156.3–157.4°C for λ_{adr} = 4–23.1), and the endotherms corresponded to the melting of the hexagonal phase.[18–20] For the higher λ_{adr} (15–23.1) in Figure 10, there were two peaks typical of commercial UHMWPE fiber product.[20] The first peak moved in the higher temperature direction with the increase of λ_{adr} from 15 to 23.1, which reflected the increase of extended chain crystal content. The second small peaks were basically at the same temperature (151–152°C) and affected by experimental operations (the sample piece lengths, etc.),[18,20,27,38] so they should be attributed to the small extent of orthorhombic–hexagonal phase transition. The relationships between the peak melting temperature, the crystallinity of the fiber samples (derived from Fig. 10), and the total draw ratio ($\lambda_{total} = \lambda_{ext} \times \lambda_{adr}$) are shown in Figure 12, where the melting temperature is the first peak temperature in Figure 10. The crystallinity was calculated by $\Delta H/\Delta H°$, taking the heat of fusion for perfect crystalline PE ($\Delta H°$) as 292.8 kJ/kg.[18] In the shrinkage measurements on the fully drawn fiber,[18] the melting point at 50% shrinkage was 140.5°C, about 2.3°C lower than the corresponding DSC temperature at a scan speed of 5°C/min. Because the fiber was allowed to relax as completely

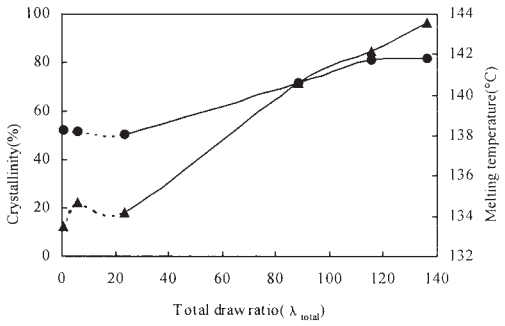

Figure 12 The (▲) melting temperature and (●) crystallinity of UHMWPE fibers (samples from experimental series 2) versus the total draw ratio ($\lambda_{total} = \lambda_{ext} \times \lambda_{adr}$).

as possible in the shrinkage experiment, this may be regarded as the closest possible approach to the equilibrium melting temperature of the fiber. Consequently, the peak melting temperature of DSC should be lowered by about 2°C to correct for the scan speed dependence of the melting temperature due to superheating.[18,39] It can be observed in Figure 12 that the as-spun fiber sample ($\lambda_{ext} = 5.9$ or $\lambda_{adr} = 1$, $\lambda_{total} = 5.9$) had lower crystallinity and a higher melting temperature compared to the free extrusion sample. The fiber sample of the first after-drawing stage ($\lambda_{ext} = 5.9$, $\lambda_{adr} = 4$, and $\lambda_{total} = 23.6$) had lower crystallinity and melting temperature compared with the as-spun fiber, which was the same result as in a previous report.[18]

Figures 13 and 14 present the equatorial and meridional WAXD scans of UHMWPE fibers (samples from experimental series 2) with different after-drawing ratios. Because the WAXD tests of the fibers were carried out at room temperature, no hexagonal phase could be found. It can be observed in Figure 13 that the (020), (200), and (110) orthorhombic reflections (~36.4°, ~24°, ~21.6°) became more and more outstanding with the increase of the after-drawing ratio. The (001) monoclinic reflections (~19.5°)[11] appeared under

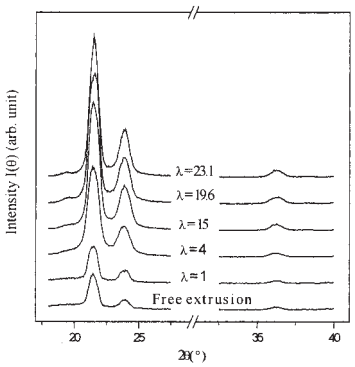

Figure 13 Equatorial WAXD scans of UHMWPE fibers (samples from experimental series 2) with different after-drawing ratios.

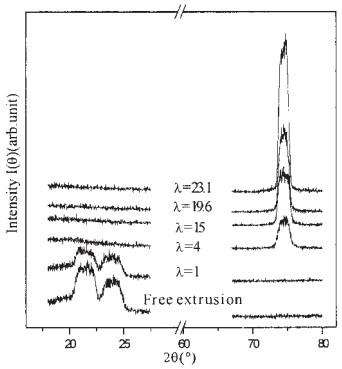

Figure 14 Meridional WAXD scans of UHMWPE fibers (samples from experimental series 2) with different after-drawing ratios.

higher after-drawing ratios. The variation tendency of the (002) orthorhombic reflection (~74.5°) in Figure 14 was nearly the same as the orthorhombic reflections in Figure 13. There still were (110) and (200) orthorhombic reflections on the meridional diffractograms for the free extrusion and draw-down samples, but they did not appear for the higher after-drawing ratio samples. From the (200), (020), and (002) orthorhombic reflections, the sizes of the *a*, *b*, and *c* axes of the orthorhombic crystal cell were calculated from the Bragg equation:

$$2d\sin\theta = n\lambda \tag{9}$$

where $n = 2$. The apparent crystal sizes along three lattice directions (perpendicular to the diffracting planes) were estimated from the Scherrer equation[18]:

$$D_{hkl} = \frac{\lambda(180/\pi)}{(H^2 - 0.01)^{1/2}\cos\theta} \tag{10}$$

where λ is the wavelength of the X-rays, θ is the Bragg angle in the corresponding (*hkl*) reflection, H is the half-width of the corresponding (*hkl*) reflection in the diffractogram, and D_{hkl} is the size of a crystallite perpendicular to its diffracting plane. The sizes of the *a*, *b*, and *c* axes of the orthorhombic crystal cell and the apparent crystal sizes D_{hkl} along three directions of the UHMWPE fibers with different after-drawing ratios are provided in Table I.

Figure 15 shows the azimuth scans under (002) orthorhombic reflections. The XRD orientation factor (f_x) was calculated from eqs. (11) and (12)[23]:

$$f_x = \frac{3\langle\cos^2\phi\rangle - 1}{2} \tag{11}$$

$$\langle\cos^2\phi\rangle = \frac{\int_0^{\pi/2} I(\phi)\sin\phi\cos^2\phi d\phi}{\int_0^{\pi/2} I(\phi)\sin\phi d\phi} \tag{12}$$

TABLE I
Sizes of *a*, *b*, and *c* Axes of Orthorhombic Crystal Cell and Apparent Crystal Sizes (D_{hkl}) Along Three Directions (Perpendicular to Diffracting Planes) of UHMWPE Fibers

After-drawing ratio	*a* Axis (nm)	D_{200} (nm)	*b* Axis (nm)	D_{020} (nm)	*c* Axis (nm)	D_{002} (nm)
Free extrusion	0.743	9.551	0.497	11.925		
1	0.743	10.088	0.495	13.270		
4	0.747	7.481	0.479	9.049	0.255	6.619
15	0.746	8.631	0.495	10.328	0.255	6.400
19.6	0.749	8.234	0.493	9.173	0.255	7.411
23.1	0.743	9.654	0.495	10.685	0.254	7.48

Figure 16 presents the relationship between the f_x and f_s of UHMWPE fibers and the after-drawing ratio. It can be observed that both f_x and f_s increased slowly in the higher after-drawing ratio region, which was not consistent with the increasing tendency of the fiber tensile properties.

It has been reported that the dichroic ratio of IR for PE could exactly reflect the orientation of the CH_2 groups, which sometimes had different results compared with the orientation of whole molecular chains.[19] Following a vibrational analysis,[19,40–42] the 1366 and 1306 cm^{-1} bands may be assigned to the kink structure (. . .*TTGTG̅TT*. . .) and the 1352 cm^{-1} band to a double gauche form (. . .TTGGTT. . .). These bands in the CH_2 wagging modes were also considered as noncrystalline bands.[43] In the CH_2 rocking region, the 731 and 720 cm^{-1} bands have been used for the measurement of crystalline orientation and average orientation.[44] Figure 17 represents the after-drawing ratio dependence of the polarized IR spectra in the frequency regions of the CH_2 rocking and wagging modes measured for the UHMWPE fibers (samples from experimental series 2). The FTIR tests of the fibers were carried out at room temperature, so there was no detectable hexagonal phase in the fiber structure. The IR dichroic absorbance (integrated intensity) ratios $A_{\parallel}/A_{\perp}$(720 and 731 cm^{-1} bands) and $A_{\parallel}/A_{\perp}$(1352 and 1366 cm^{-1} bands), based on Figure 17, are shown in Figure 18. It can be observed that, with the increase of the after-drawing ratio, the $A_{\parallel}/A_{\perp}$(720 + 731 cm^{-1}) curve declined quickly at the beginning and then slowly in the region of the high after-drawing ratio, which reflected the rising tendency of the average orientation and corresponded to the variation tendency of the f_s. The $A_{\parallel}/A_{\perp}$(1352 + 1366 cm^{-1}), which reflected the orientation of the CH_2 groups in folded chains, increased with the increase of the after-drawing ratio except for the final point. The reason for the abrupt decrease at the final point might be that the last stage after-drawing was under a temperature (140°C) close to the equilibrium melting temperature (140.5°C) for fully drawn UHMWPE fiber[18]: under this high temperature and high drawing tension the migration of crystal defects into amorphous regions occurred.[5] Some chain ends might exist in the crystalline regions, because they did not lead to a serious distortion of the crystal lattice.[45] During the migration of crystal defects, some of these chain ends might be pulled out of the crystalline region, and their recoiling would result in an abrupt decrease of the CH_2 group orientation in folded chains at the final point in Figure 18. Figure 19 presents the after-drawing ratio dependence of the unpolarized IR spectra in the frequency regions of the CH_2 wagging and bending modes. In the CH_2 bending region, the 1473 and 1463 cm^{-1} bands have been used for the measurement of crystal-

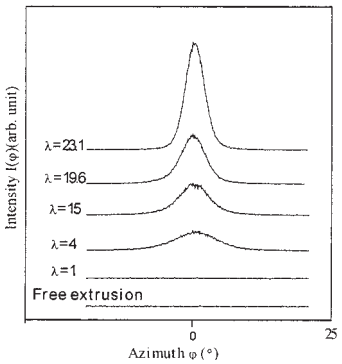

Figure 15 An azimuthal scanning profile for the meridional (002) peak of UHMWPE fibers (samples from experimental series 2) with different after-drawing ratios.

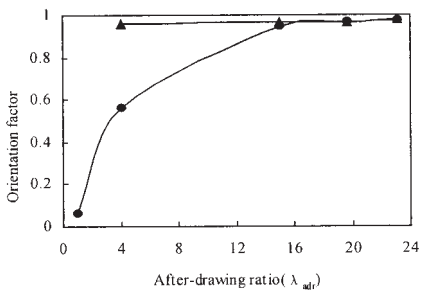

Figure 16 The (▲) X-ray diffraction orientation factor (f_x) and (●) sonic velocity orientation factor (f_s) of UHMWPE fibers (samples from experimental series 2) versus the after-drawing ratio.

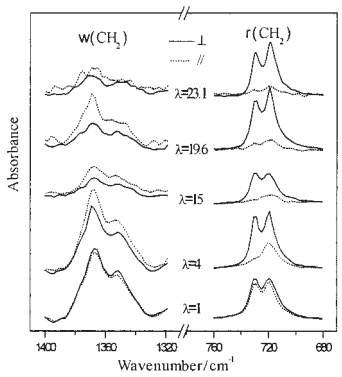

Figure 17 The after-drawing ratio dependence of the polarized IR spectra in the frequency regions of the CH_2 rocking and wagging modes measured for the UHMWPE fibers (samples from experimental series 2). The symbols indicate that the electric vector of the incident IR beam was perpendicular (⊥) and parallel (‖) to the chain orientation direction.

line orientation and average orientation.[46] The A(1352 and 1366 cm^{-1} bands)/A(1463 and 1473 cm^{-1} bands) ratios may reflect the relative content of folded chains, and they are shown in Figure 20 together with taut tie molecules (TTM) fractions of the UHMWPE fiber samples. The TTM fraction (β) was calculated from eq. (13)[47]:

$$E = E_c \times \frac{1 + (1 - x)/(x - \beta)}{1 + (1/\beta) \times (1 - x)/(x - \beta)} \qquad (13)$$

where E_c represents the theoretical modulus of PE, E represents the modulus of the fiber that is found in tensile testing, and x represents the crystallinity (derived from DSC). From spectroscopic techniques, the theoretical modulus of PE is estimated as 350 GPa.[48] It can be observed in Figure 20 that the increase of the TTM fraction and the decrease of the A(1352 + 1366 cm^{-1})/A(1463 + 1473 cm^{-1}) ratio corresponded to each other except at the final point. The abrupt increase of the A(1352 + 1366 cm^{-1})/A(1463 + 1473 cm^{-1}) ratio, which might be for the same reason as the abrupt decrease of $A_{\|}/A_{\perp}$(1352 + 1366 cm^{-1}) at the final point in Figure 18 mentioned above, did not influence the increase of the TTM fraction, because the ratio only represents the fraction of the folded chains.

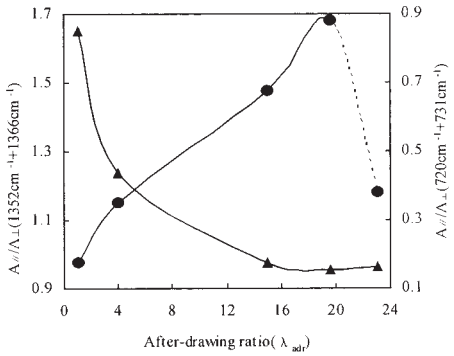

Figure 18 The IR dichroic ratios (▲) $A_{\|}/A_{\perp}$(720 + 731 cm^{-1}) and (●) $A_{\|}/A_{\perp}$(1352 + 1366 cm^{-1}) of UHMWPE fibers (samples from experimental series 2) versus the after-drawing ratio.

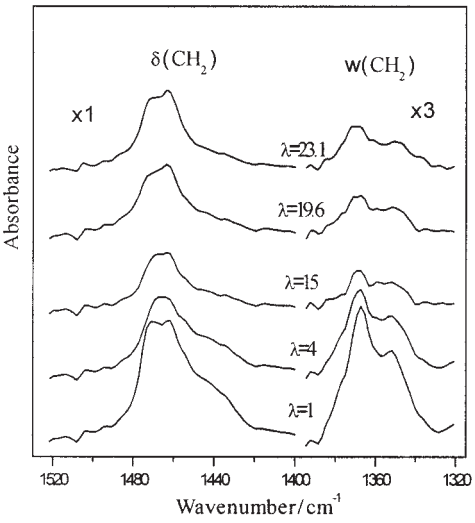

Figure 19 The after-drawing ratio dependence of the unpolarized IR spectra in the frequency regions of the CH_2 wagging and bending modes measured for the UHMWPE fibers (samples from experimental series 2).

CONCLUSIONS

An optimum draw-down ratio was found in the multihole dry spinning process of UHMWPE/decalin solution, which may be explained by molecular disen-

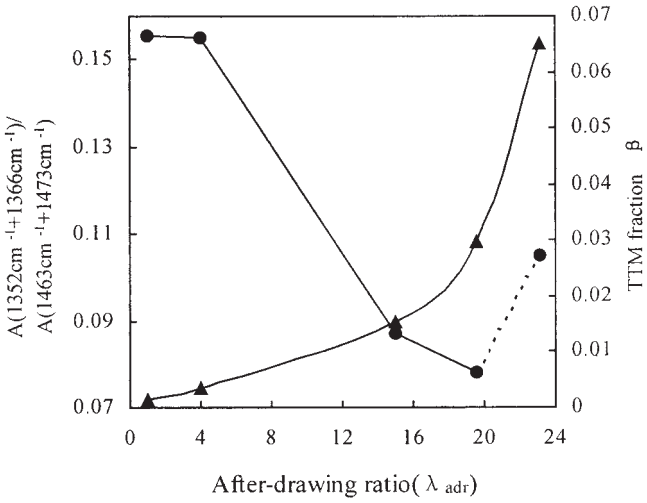

Figure 20 The (●) A(1352 + 1366 cm^{-1})/A(1463 + 1473 cm^{-1}) and (▲) taut tie molecules (TTM) fraction (β) of UHMWPE fibers (samples from experimental series 2) versus the after-drawing ratio.

tanglement and the composite effect of entropy and viscosity components. The as-spun fiber by draw-down had an obvious shish kebab morphology, lower crystallinity, and higher melting temperature compared with a free extrusion sample, and higher crystallinity and melting temperature compared with the fiber by first-stage after-drawing. During the subsequent after-drawing process, the crystallinity, melting temperature, XRD, and sonic velocity orientation factors (f_x and f_s) increased slowly in the higher after-drawing ratio region, which is not consistent with the increasing trend of the tensile properties. The polarized and unpolarized IR spectra reflected the variations of the orientation and the content of the folded chains.

References

1. Ohta, Y. Sen'i Gakkaishi 1999, 55, 413.
2. Smith, P.; Lemstra, P. J. Colloid Polym Sci 1980, 258, 891.
3. Lemstra, P. J.; van Aerle, N. A. J. M.; Bastiaansen, C. W. Polym J 1987, 19, 85.
4. Smith, P.; Lemstra, P. J. Makromol Chem 1979, 18, 2983.
5. Kalb, B.; Pennings, A. J. J Mater Sci 1980, 15, 2584.
6. Smith, P.; Lemstra, P. J.; Pijpers, J. P. L.; Kiel, A. M. Colloid Polym Sci 1981, 259, 1070.
7. Smith, P.; Lemstra, P. J.; Booij, H. C. J Polym Sci Polym Phys Ed 1981, 19, 877.
8. Graessley, W. W. Adv Polym Sci 1974, 16, 58.
9. Kavesh, S. Honeywell International Inc., WO 01/73173 A1, World Intellectual Property, 2001.
10. Sun, Y. China Petrochemical Company and China Textile Academy, CN Pat. 1,400,342A (2003).
11. Xiao, C.; Zhang, Y.; An, S.; Jia, G. J Appl Polym Sci 1996, 59, 931.
12. Xiao, C.; An, S.; Jia, G.; Zhang, Y. Acta Polym Sin 1999, 2, 171.
13. Xiao, C.; An, S.; Jia, G.; Zhang, Y. Text J (China) 1997, 18, 11.
14. Chen, Z.; Liu, Z.; Hu, Z. J Chin Text Univ 1992, 18, 12.
15. Pan, L.; Hu, Z.; Liu, Z.; Zhang, A.; Wu, Z. J Chin Text Univ 1991, 17, 53.
16. Zhang, A.; Chen, K.; Lu, P.; Hu, Z.; Wu, Z. Synth Fiber Ind (China) 1988, 11, 23.
17. Pennings, A. J.; Roukema, M.; Van der Veen, A. Polym Bull 1990, 23, 353.
18. Smook, J.; Pennings, J. Colloid Polym Sci 1984, 262, 712.
19. Tashiro, K.; Sasaki, S.; Kobayashi, M. Macromolecules 1996, 29, 7460.
20. Tsubakihara, S.; Nakamura, A.; Yasuniwa, M. Polym J 1996, 28, 489.
21. Zhang, Y.; Xiao, C.; Jia, G.; An, S. J Appl Polym Sci 1999, 74, 670.
22. Pennings, A. J.; Smook, J.; de Boer, J.; Gogolewski, S.; van Hutten, P. F. Pure Appl Chem 1983, 55, 777.
23. Liang, B. R.; Qu, F. Z.; Pan, L. H.; Liu, X. J.; Wu, C. X. In Polymer Physics; Liang, B. R., Ed.; China Textile Press: Beijing, 2000; Chapter 8.
24. Brereton, M. G.; Klein, P. G. Polymer 1988, 29, 970.
25. Edwards, S. F.; Vilgis, Th. Polymer 1986, 27, 483.
26. Ball, R. C.; Doi, M.; Edwards, S. F.; Warner, M. Polymer 1981, 22, 1010.
27. Pan, L.; Liu, Z.; Hu, Z.; Zhu, J.; Zhang, A.; Wu, Z. Polym Mater Sci Eng (China) 1993, 3, 89.
28. Pennings, A. J.; Zwijnenburg, A. J Polym Sci Polym Phys Ed 1979, 17, 1011.
29. van Aerle, N. A. J. M.; Lemstra, P. J. Polym J 1988, 20, 131.
30. Kyotani, H.; Tanabe, Y. Kobunshi Ronbunshu 1989, 46, 51.
31. van Aerle, N. A. J. M.; Lemstra, P. J.; Braam, A. W. M. Polym Commun 1989, 30, 7.
32. Murthy, N. S.; Correale, S. T.; Kavesh, S. Polym Commun 1990, 31, 50.
33. Westrum, Jr., E. F.; Mc Cullough, J. P. In Physics and Chemistry of the Organic Solid State; Fox, D.; Labes, M. M.; Weissberger, A., Eds.; Wiley: New York, 1963; Vol. 1.
34. Ungar, G.; Keller, A. Polymer 1980, 21, 1273.
35. Clough, S. B. J Macromol Sci 1970, B4, 199.
36. Bassett, D. C.; Block, S.; Piermarini, G. J Appl Phys 1974, 45, 4146.
37. Uehara, H.; Kanamoto, T.; Kawaguchi, A.; Murakami, S. Macromolecules 1996, 29, 1540.
38. Hu, Z.; Yu, J.; Liu, Z.; Liu, J. Synth Fiber Ind (China) 2000, 23, 13.
39. Zachmann, H. G. Koll Zu Z Polym 1965, 206, 25.
40. Snyder, R. G.; Maroncelli, M.; Qi, S. P.; Strauss, H. L. Science 1981, 214, 188.
41. Maroncelli, M.; Qi, S. P.; Strauss, H. L.; Snyder, R. G. J Am Chem Soc 1982, 104, 6327.
42. Kim, Y.; Strauss, H. L.; Snyder, R. G. J Phys Chem 1989, 93, 7520.
43. Tabb, D. L.; Sevcik, J. J.; Koenig, J. L. J Polym Sci Polym Phys Ed 1975, 13, 815.
44. Stein, R. S. J Polym Sci 1958, 31, 327.
45. Predecki, P.; Statton, W. Appl Polym Symp 1967, 6, 165.
46. Uemura, Y.; Stein, R. S. Appl Polym Symp 1972, 10, 1691.
47. Penning, J. P.; van der Werff, H.; Roukema, M.; Pennings, A. J. Polym Bull 1990, 23, 347.
48. Fanconi, B.; Rabolt, J. R. J Polym Sci Polym Phys Ed 1985, 23, 1201.